NASA Technical Memorandum 105773

Analysis of Iced Wings

T. Cebeci, H.H. Chen, K. Kaups, S. Schimke
California State University, Long Beach
Long Beach, California

and

J. Shin
Lewis Research Center
Cleveland, Ohio

Prepared for the
30th Aerospace Sciences Meeting and Exhibit
sponsored by the American Institute of Aeronautics and Astronautics
Reno, Nevada, January 6–9, 1992

NASA

ANALYSIS OF ICED WINGS

Tuncer Cebeci*, H. H. Chen**, K. Kaups†, S. Schimke††
Aerospace Engineering Department
California State University, Long Beach
and
Jaiwon Shin†††
NASA Lewis Research Center

Abstract

A method for computing ice shapes along the leading edge of a wing and a method for predicting its aerodynamic performance degradation due to icing is described. Ice shapes are computed using an extension of the LEWICE code which was developed for airfoils. The aerodynamic properties of the iced wing are determined with an interactive scheme in which the solutions of the inviscid flow equations are obtained from a panel method and the solutions of the viscous flow equations are obtained from an inverse three-dimensional finite-difference boundary-layer method. A new interaction law is used to couple the inviscid and viscous flow solutions.

The application of the LEWICE wing code to the calculation of ice shapes on a MS-317 swept wing show good agreement with measurements. The interactive boundary-layer method is applied to a tapered iced wing in order to study the effect of icing on the aerodynamic properties of the wing at several angles of attack.

1.0 Introduction

The National Aircraft Icing Technology Plan[1] called for the creation of a method to simulate ice accretion on an aircraft and predict the effect of ice accretion on aircraft performance. This paper presents results which suggest that the realization of this goal is within reach, largely due to the technical and organizational abilities of NASA Lewis Research Center, which developed the LEWICE code for the calculation of ice-accretion on airfoils as a function of atmospheric conditions[2,3] and supported the development of methods to determine the resulting aerodynamic properties of iced airfoils and wings.[4-6] At the same time, the NASA Lewis Research tunnel has been used for the study of the process of ice formation, and an experimental program has been initiated to measure degradation of the aerodynamic performance of airfoils[7] and wings.[8] It is intended that the resulting simulation method, which will solve the conservation equations and predict ice accretion, will be evaluated by comparing the results of these calculations with experimental data. This method will then be used to assist in the prediction of the performance degradation of wings in icing conditions and thereby assist in ensuring that the Regulations of the Federal Aviation Authority[9] are met.

Research on aircraft icing can be judged in many ways; for example, by the presentations made to the Icing Workshop held at NASA Lewis Research Center annually and by the several papers presented each year at the AIAA Aerospace Sciences Meeting. The experimental investigation of Bragg et al.[10], in which the effects of simulated accretions of glaze ice were measured on a wing with a NACA 0012 airfoil cross-section, follows from a series of earlier valuable contributions.[11-13] Numerical investigations have already begun to consider fixed and rotary wing performance (i.e. Kwon and Sankar[14,15]). A major requirement, however, is to extend the LEWICE code to the representation of ice shapes on the leading edge of a wing and combine it with a method for the determination of performance, and to do so for three-dimensional flows over complete airframes and at a modest cost so that the implications of aircraft geometry, angle of attack, speed, and atmospheric conditions can be predicted. It is self-evident that this achievement will be of value only if the components of the simulation method as well as the full simulation method in its entirety are tested and the results compared with experimental data.

It is generally accepted that the variation of the shapes of ice with atmospheric conditions which lead to rime ice can be determined on airfoils with the current version of the LEWICE code and that the shape of glaze ice, although acceptable, can and should be improved.[16,17] In this work it is assumed that the LEWICE code is the best available, generally satisfactory, and amenable to improvement. Thus, the problem is to develop a three-dimensional version of the LEWICE code and combine it with a three-dimensional method for the determination of aerodynamic properties, taking into account the fact that ice formations are neither continuous nor smooth. Since one of the main components of the present computer method to predict ice shapes is a method for the solution of inviscid-flow equations, it would be advantageous if this approach could also be used for the prediction of aerodynamic properties of iced wings.

It can be envisaged, at least by those with a long-term view, that the Reynolds-averaged Navier-Stokes equations might provide the basis for the prediction of aerodynamic properties, and scrutinizing the related literature on the solution of two-dimensional equations for smooth airfoils reveals that there is a dichotomy of view. It would seem, however, that even these comparatively simple flows are investigated using equations that are further reductions of the Navier-Stokes equations, including thin-layer Navier-Stokes equations and by the interaction of inviscid and boundary-layer equations. The former approach, like those

* Professor and Chairman. Fellow AIAA.
** Associate Professor. Senior Member AIAA.
† Research Professor. Member AIAA.
†† Research Associate.
††† Aerospace Engineer. Member AIAA.

with higher-order equations, holds much promise, but the cost of computation - even in two dimensions - is large and becomes prohibitive for use in three dimensions, particularly with complete aircraft geometries. For the foreseeable future the interactive approach is to be preferred. The inviscid-flow procedure may be identical to that already utilized within the LEWICE code so that the ice accretion may be part of an interactive calculation.

The interactive method used in this paper has been widely used for two-dimensional flows, so its prediction abilities are known for a wide range of smooth body shapes, iced airfoils, and aerodynamic and atmospheric conditions. In addition, it has recently been applied to wings[18] and, although further developments are desirable to determine a more efficient means of achieving the inviscid-viscous interaction in three-dimensional flows, it is clearly able to deal with wing geometries and potentially complete aircraft. In this paper, we describe a general procedure for predicting ice shapes on wings and determining their influence on the aerodynamic properties of the wings. This procedure incorporates a general inviscid code developed by Hess.[19]

This paper describes the extension to wing flows of the combined LEWICE/IBL procedure developed for airfoils. Section 3 describes the procedure developed for calculating ice shapes along the leading edge of a wing. Section 4 describes the interactive boundary-layer method for computing three-dimensional flows on iced wings. In both sections, use is made of Hess's three-dimensional panel method for computing the inviscid flowfield as described in Section 2. Section 5 presents a comparison between calculated and measured iced shapes obtained under infinite swept wing conditions on a MS-317 swept wing. The results of Section 6 show the influence of 390 and 1164-second rime ice on the performance degradation of a NACA 0012 tapered wing at several angles of attack. In this case, the interactive boundary-layer calculations were performed for a prescribed ice shape distribution along the wing leading edge using the procedure described in Section 4. The paper ends with a brief discussion of the implications of the work and a summary of the more important conclusions.

2.0 Three-Dimensional Panel Method

We use the surface-source panel method developed by Hess[19] for computing the inviscid flow about a complete airplane configuration. This method represents a general body by a set of quadrilateral panels as shown in Fig. 1. A three-dimensional configuration in general consists of lifting sections, such as a wing or pylon for which there is a well-defined trailing edge, and nonlifting sections, such as the fuselage. Under the formulation adopted by Hess, all panels are assigned an independent source distribution, while those on a lifting section are assumed to carry a bound vorticity distribution. The variation of this bound vorticity in the streamwise direction is assumed, while its variation in the spanwise direction is adjusted to satisfy the Kutta condition at the trailing edge. The complete solution for a prescribed flow condition is obtained by simultaneously satisfying a condition of zero normal velocity at a control point on each panel of

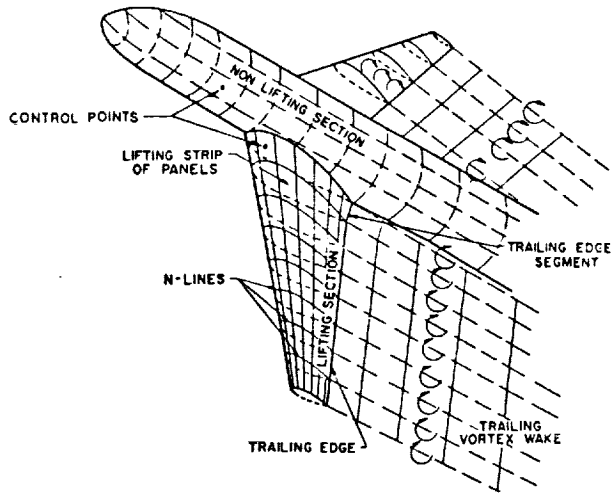

Fig. 1. Wing/body configuration.

the body together with a Kutta condition at each trailing-edge panel.

The nature of the Kutta condition varies greatly among the many panel methods which are currently available. While the Kutta condition adopted by Hess assumed equal upper and lower surface pressures at the trailing edge, other methods make use of other derived conditions that do not guarantee a pressure match at the trailing edge. For instance, Margason et al.[20] showed that pressure mismatches of up to half of the free-stream dynamic pressure could occur from such alternate forms of the Kutta condition. Since we are also interested in the computation of inviscid flows with viscous effects, and since the behavior of the boundary-layer at the trailing edge can have a significant effect on the overall solution, it is believed that the approach adopted here is more realistic and blends in well with the previous studies on two-dimensional flows employing interaction procedures.

3.0 Three-Dimensional Ice Shapes and Their Calculation

Before we describe our procedure for calculating the ice shapes along the leading edge of a wing for given atmospheric conditions, it is useful to review the ice accretion procedure used in the LEWICE program for airfoils. LEWICE consists of three main modules: (1) prediction of inviscid flow by a panel method, (2) calculation of the trajectories of water droplets driven by the air velocities so that the impingement pattern of the water droplets on the surface can be determined, and (3) a quasi-steady-state surface heat transfer analysis in which mass and energy equations are solved for a two-dimensional flow in order to determine the ice shape. As discussed in Ref. 3, the heat balance equation for a control volume includes terms providing heat to or removing heat from the control volume. The dominant "heat removal" term is due to convective cooling and the dominant heat source term is due to the heat released by the freezing of water entering the control volume. The water entering a control volume consists of: (1) water droplets impinging on the airfoil surface, and (2) water "running back" from an adjacent upstream control volume.

The above procedure for airfoils has been found to be remarkably good for predicting ice shapes, (see for example Ref. 17) despite the very empirical nature of the expressions used in the heat balance as well as in the physical model of the ice accretion process. Studies conducted by Olsen and Walker[21,22] show that at aircraft speeds there is no flow of liquid over the surface of the ice after a short initial flow, even at subfreezing temperatures that are close to the freezing point. Instead, there are very large stationary drops on the ice surface that lose water from their bottoms by freezing as water is added to the droplets by the addition of microscopic cloud droplets. This observation disagrees with the existing physical model used in the LEWICE code, since it assumes that there is a thin liquid continuously flowing over the ice surface. While this model disagrees with the experimental evidence, especially for conditions leading to horn-shaped clear (glaze) ice, it does reasonably well for rime ice which forms when the air temperature is low enough to cause the cloud droplets to freeze almost immediately on impact.

The role that the liquid layer plays in the formation of glaze ice has been further elaborated on by Hansman and Turnock[23] and Bilanin[24], who point to the surface tension phenomenon as the most likely source for the observed deviations. There is convincing evidence from tests with variable surface tension that ice growth depends on it. Although a smooth water film may form at the stagnation point, it soon breaks up by the beading process and freezes into irregular rough lumps that enhance heat transfer and speed up the ice growth. The parameters controlling transition from a smooth film to beads and to rough ice formation are not well known at this time. For this reason, care is required to extend the ice accretion procedure from two- to three- dimensional flows.

In principle, the extension of the LEWICE airfoil procedure to three-dimensional flows requires that the trajectory calculations be performed for the three components of the velocity obtained from a three-dimensional panel method and a heat transfer balance which also includes the spanwise direction. While the former can be done with increased computer cost, the latter is difficult in view of the empirical nature of the heat transfer coefficient, h_c, used to represent the convective cooling. In the present LEWICE program, this parameter for turbulent flows is expressed by

$$h_c = \left[\frac{c_f/2}{Pr_t + \sqrt{(c_f/2)}\ (1/St_k)}\right] \rho u_e c_p \qquad (1)$$

through the Reynolds analogy with local skin-friction coefficient, c_f, given by an expression valid for a flat-plate flow with roughness,

$$\frac{c_f}{2} = \left\{\frac{0.41}{\ln\left[864\ (\theta_t/k_s) + 2.568\right]}\right\}^2 \qquad (2)$$

The parameter St_k represents a dimensionless roughness parameter given by

$$St_k = 1.16\ \left(\frac{u_\tau k_s}{\nu}\right)^{-0.2} \qquad (3)$$

The momentum thickness, θ_t, is calculated by a momentum integral method which employs a smooth flat-plate skin-friction coefficient as one of the auxiliary equations necessary to solve the integral equation. Since Eq. (1) is based mainly on data correlation with roughness parameters chosen so that the computed ice shapes fit the experimental data, any attempt to add a spanwise heat transfer coefficient to the heat balance equation will be empirical and can only be done where experimental data exists. As a first step, however, it is prudent to leave the heat balance in its two-dimensional form and assume it to apply to a three-dimensional body which is expressed in an equivalent two-dimensional form. One approach, followed by Potapczuk and Bidwell[25], is to perform the trajectory calculations for a three-dimensional flowfield by determining the impingement patterns of the water droplets resulting from the three components of the velocity field and apply this along the streamlines on the wing. Another approach, followed here, is to approximate the 3D wing by an equivalent yawed infinite wing at each spanwise station. In this case, the flowfield can be calculated by a three-dimensional panel method and the particle trajectories calculated in a quasi-three-dimensional manner, so that the two-dimensional heat balance can be applied along the airfoil section normal to the leading edge of the wing. Each approach has its advantages and must be evaluated against experimental data. Studies reported by Potapczuk and Bidwell show that their approach leads to ice shapes which are in good agreement with experimental data.

It is also useful to seek other approaches to extend the two-dimensional ice accretion model to three-dimensional flows since the computer cost of predicting an ice shape at a given spanwise section is relatively high. For example, the approach of Potapczuk takes about 20 minutes on a Cray, while the present approach takes less than 7 minutes. If the wing is approximated, say by ten airfoil sections, then the use of the computer program to predict the ice shapes along the leading edge of a wing can require between one and three hours. It is also possible that the dominant effect lies with the heat transfer balance and that "more accurate" trajectory calculations may not have an appreciable effect on the ice shapes. The answers to all these questions, however, can be provided by comparing the calculated ice shapes with experimental data.

3.1 Present Approach for Calculating Ice Shapes on Wings

To describe our approach, which is based on the extension of the LEWICE airfoil code to wings, we use the three-dimensional panel method described in Section 2. For a wing defined by streamwise cross-sections, we calculate the velocity components $V_{\bar{x}}$, $V_{\bar{y}}$, $V_{\bar{z}}$ in a Cartesian coordinate system x, y, z at a specified incidence angle α measured from the x-axis. If we denote the unit vectors in this coordinate system by ($\hat{e}_1$, $\hat{e}_2$, $\hat{e}_3$), then the velocity vector can be written as

$$\vec{V} = V_{\bar{x}}\hat{e}_1 + V_{\bar{y}}\hat{e}_2 + V_{\bar{z}}\hat{e}_3 \qquad (4)$$

We now approximate the wing by an equivalent yawed infinite wing at each spanwise station. For this purpose, we define a new Cartesian coordinate system (x,y,z) constructed so that x is normal to the leading edge of the wing and y is normal to the airfoil chord c_n. If we let α_t represent the local incidence angle of the chord c with respect to the x-axis, as shown in Fig. 2, with a and b denoting

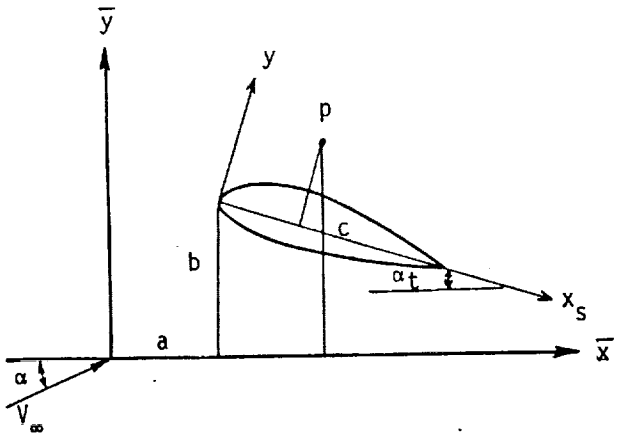

Fig. 2. Definitions for a streamwise cut of a wing.

the leading edge of the chord line, then it can be shown that for an airfoil section defined normal to the leading edge $(x/c_n, y/c_n)$ the relationship between the $(\bar{x},\bar{y})$ and (x,y) coordinates can be expressed by

$$\frac{\bar{x}}{c} = \frac{a}{c} + \frac{c_n}{c}\frac{[(x/c_n)\cos\alpha_n + (y/c_n)\sin\alpha_n]}{\cos\lambda} \quad (5a)$$

$$\frac{\bar{y}}{c} = \frac{c_n}{c}\left[\frac{b}{c_n} - \frac{x}{c_n}\sin\alpha_n + \frac{y}{c_n}\cos\alpha_n\right] \quad (5b)$$

Here α_n corresponds to the local incidence angle of the chord c_n with respect to the $\bar{x}_n$-axis, which represents the coordinate normal to the leading edge defined in the (x,z) plane. α_n is related to α_t and λ by

$$\tan\alpha_n = \frac{\tan\alpha_t}{\cos\lambda} \quad (6a)$$

The relation between the airfoil chord length normal to the leading edge of the wing and the streamwise airfoil chord length is

$$c_n = \frac{\cos\alpha_t\cos\lambda}{\cos\alpha_n}\,c \quad (6b)$$

The trajectory calculations require that the velocity components in three directions are given and, since the panel method computes the velocities for the (x,y,z) coordinate system, it is necessary to determine them in the (x,y,z) coordinate system so that ice accretion can be computed on an equivalent two-dimensional model. If we denote the unit vectors of the coordinate system (x,y,z) by $(\hat{i},\hat{j},\hat{k})$, then the relationship between the unit vectors in the two coordinate systems are

$$\hat{i} = \hat{e}_1\cos\alpha_n\cos\lambda - \hat{e}_2\sin\alpha_n - \hat{e}_3\cos\alpha_n\sin\lambda \quad (7a)$$

$$\hat{j} = \hat{e}_1\sin\alpha_n\cos\lambda + \hat{e}_2\cos\alpha_n - \hat{e}_3\sin\alpha_n\sin\lambda \quad (7b)$$

$$\hat{k} = \hat{e}_1\sin\lambda + \hat{e}_3\cos\lambda \quad (7c)$$

Each velocity component, V_x, V_y, V_z, in the (x,y,z) coordinate system can be obtained by taking a dot product of the velocity vector $\bar{V}$ with its respective unit vector, that is,

$$V_x = \bar{V}\cdot\hat{i} = V_{\bar{x}}\cos\alpha_n\cos\lambda - V_{\bar{y}}\sin\alpha_n - V_{\bar{z}}\cos\alpha_n\sin\lambda \quad (8a)$$

$$V_y = \bar{V}\cdot\hat{j} = V_{\bar{x}}\sin\alpha_n\cos\lambda + V_{\bar{y}}\cos\alpha_n - V_{\bar{z}}\sin\alpha_n\sin\lambda \quad (8b)$$

$$V_z = \bar{V}\cdot\hat{k} = V_{\bar{x}}\sin\lambda + V_{\bar{z}}\cos\lambda \quad (8c)$$

Similarly, for a freestream velocity given by

$$\bar{V}_\infty = V_\infty[\hat{e}_1\cos\alpha + \hat{e}_2\sin\alpha] \quad (9)$$

the components of the freestream velocity in the (x,y,z) directions are:

$$(V_x)_\infty = \bar{V}_\infty\cdot\hat{i} = V_\infty[\cos\alpha\cos\alpha_n\cos\lambda - \sin\alpha_n\sin\alpha] \quad (10a)$$

$$(V_y)_\infty = \bar{V}_\infty\cdot\hat{j} = V_\infty[\cos\alpha\sin\alpha_n\cos\lambda + \cos\alpha_n\sin\alpha] \quad (10b)$$

$$(V_z)_\infty = \bar{V}_\infty\cdot\hat{k} = V_\infty[\cos\alpha\sin\lambda] \quad (10c)$$

Since our model is for a yawed infinite wing, then V_z given by Eq. (8c) and $(V_z)_\infty$ by Eq. (10c) must be equal. This leads to the relation

$$V_{\bar{z}} = V_\infty\tan\lambda\cos\alpha - V_{\bar{x}}\tan\lambda \quad (11)$$

which allows the expressions given by Eq. (8) to be expressed in the following forms

$$V_x = V_{\bar{x}}\frac{\cos\alpha_n}{\cos\lambda} - V_{\bar{y}}\sin\alpha_n - V_\infty\frac{\cos\alpha_n\cos\alpha\sin^2\lambda}{\cos\lambda} \quad (12a)$$

$$V_y = V_{\bar{x}}\frac{\sin\alpha_n}{\cos\lambda} + V_{\bar{y}}\cos\alpha_n - V_\infty\frac{\sin\alpha_n\cos\alpha\sin^2\lambda}{\cos\lambda} \quad (12b)$$

$$V_z = V_\infty\cos\alpha\sin\lambda \quad (12c)$$

with total velocity V_T given by,

$$V_T^2 = (V_x^2 + V_y^2 + V_z^2) = V_{\bar{x}}^2 + V_{\bar{y}}^2 + (V_\infty\cos\alpha - V_{\bar{x}})^2\tan^2\lambda \quad (13)$$

The trajectory calculations for an airfoil section in a plane normal to the leading edge of the wing are similar to those for a two-dimensional flow. Instead of solving two equations of motion in the x and y directions, we now need to consider three equations in the x,y and z directions even though the particle paths are calculated only in a plane normal to the leading edge of the wing according to the model discussed previously. To elaborate on this point further, we use the trajectory analysis discussed in Ref. 3 and apply appropriate modifications to incorporate our equivalent infinite swept wing approach into the two-dimensional analysis.[3]

Let us consider a water particle in a flowfield where the freestream velocity makes an angle β with the x-axis, as shown in Fig 3. The (x,y) coordinate system represents the airfoil coordinate

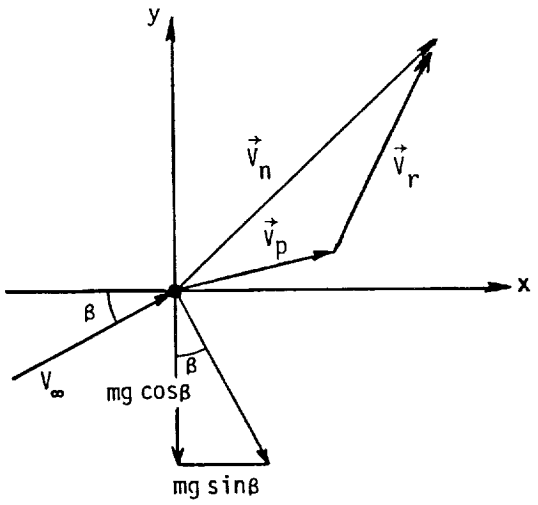

Fig. 3. Water particle velocities.

system with $\vec{V}_n$ denoting the local total velocity to which the particle is subjected and is computed by the panel method. The particle velocity is denoted by $\vec{V}_p$ and the relative air velocity that the particle experiences by

$$\vec{V}_r = \vec{V}_n - \vec{V}_p \tag{14}$$

where

$$\vec{V}_n = V_x\hat{i} + V_y\hat{j} \tag{15a}$$

$$\vec{V}_p = V_{px}\hat{i} + V_{py}\hat{j} = \frac{dx_p}{dt}\hat{i} + \frac{dy_p}{dt}\hat{j} \tag{15b}$$

From Eqs. (14) and (15b), the relative air velocity with respect to the moving particle can be expressed as,

$$\vec{V}_r = (V_x - V_{px})\hat{i} + (V_y - V_{py})\hat{j} \tag{16}$$

so that the unit vector, $\hat{e}_r$, in the $\vec{V}_r$ direction can be computed by

$$\hat{e}_r = \frac{\vec{V}_r}{|V_r|} = \frac{V_x - V_{px}}{V_r}\hat{i} + \frac{V_y - V_{py}}{V_r}\hat{j} \tag{17}$$

We now apply Newton's law of motion to the particle in the e_r-direction. Neglecting the lift force, the forces acting on the particle correspond to the drag force, $\vec{F}_a$, and gravitational force, $\vec{F}_g$, so that with $\vec{r}_p = x\hat{i} + y\hat{j}$ and with m denoting the particle mass,

$$m\frac{d^2\vec{r}_p}{dt^2} = \vec{F}_a + \vec{F}_g \tag{18}$$

where

$$\vec{F}_a = \hat{e}_r C_d \rho \frac{V_r^2}{2} A_p \tag{19a}$$

$$\vec{F}_g = mg(\hat{i}\sin\beta - \hat{j}\cos\beta) \tag{19b}$$

Here C_d is the drag coefficient, ρ the density of air, A_p the cross-sectional area perpendicular to the flow, and g the acceleration of gravity.

Resolving Eq. (18) into its components and using the solutions in Eq. (19), we can write

$$\frac{d^2x_p}{dt^2} = \frac{C_d\rho A_p}{2m} V_r(V_x - V_{px}) + g\sin\beta \tag{20a}$$

$$\frac{d^2y_p}{dt^2} = \frac{C_d\rho A_p}{2m} V_r(V_y - V_{py}) - g\cos\beta \tag{20b}$$

$$\frac{d^2z_p}{dt^2} = \frac{C_d\rho A_p}{2m} V_r[V_z - V_{pz}] \tag{20c}$$

where

$$V_{pz} = \frac{dz_p}{dt} \tag{21}$$

If we now include the components of the particle and inviscid air velocities in the $\hat{k}$-direction in the definition of the relative air velocity $\vec{V}_r$ with respect to the moving particle, we can write the resulting relative air velocity as

$$\vec{V}_r = (V_x - V_{px})\hat{i} + (V_y - V_{py})\hat{j} + (V_z - V_{pz})\hat{k} \tag{22}$$

If we now invoke the yawed infinite swept wing assumption which requires that the spanwise inviscid velocity component V_z is constant, then we can write

$$V_z = V_\infty \sin\lambda \cos\alpha \tag{23}$$

With this assumption, we note that with $A = C_d\rho A_p/2m$, Eq. (20c) is of the form

$$\frac{dV_{pz}}{V_z - V_{pz}} = AV_r dt \equiv dG \tag{24}$$

since

$$\frac{dV_{pz}}{dt} = \frac{d^2z_p}{dt^2}$$

Assuming that the right-hand side of Eq. (24) is a function of t only, we can integrate Eq. (24) and write the resulting expression in the form

$$V_{pz} = V_z - (V_z - V_{pz}^1)e^{-G(t)} \tag{25}$$

where V_{pz}^1 denotes the particle release velocity. Equation (25) shows that if the particle is released with a speed equal to the total inviscid velocity, then the spanwise velocity component of the particle is equal to the inviscid spanwise velocity which is constant. As a result, the relative air velocity for a yawed infinite swept wing, Eq. (22), is the same as that for a two-dimensional flow, Eq. (20). This means that the expressions used in trajectory calculations for two-dimensional flows can also be used for finite swept wings when the flowfield is computed by a three-dimensional panel method and the spanwise velocity component is assumed to be fixed by a yawed wing approximation.

4.0 Three-Dimensional Interactive Boundary-Layer Method

As in two-dimensional flows, the interactive method for three-dimensional flows is based on the solutions of the inviscid and boundary-layer

equations. An interface program, illustrated by Fig. 4, is placed between the inviscid and three-dimensional inverse boundary-layer methods to process the geometry and inviscid velocity data for input to the boundary-layer program. The basic input to this program is (1) the definition of the wing configuration that is used by a geometry subroutine to construct a nonorthogonal coordinate system and (2) the associated geometrical parameters, which consist of the geodesic curvatures and metric coefficients needed in the boundary-layer calculations. Some of the generated data is used later in a velocity subroutine to determine the inviscid velocity components at the boundary-layer grid points and to transform the inviscid velocity components on the surface, calculated in a Cartesian coordinate system, into the boundary-layer coordinate system. This operation consists of calculating dot products of velocity vectors as well as chordwise and spanwise interpolation. Further velocity and geometry data processing is carried out in a subroutine that separates the generated information into upper and lower surfaces of the wing for boundary-layer calculations.

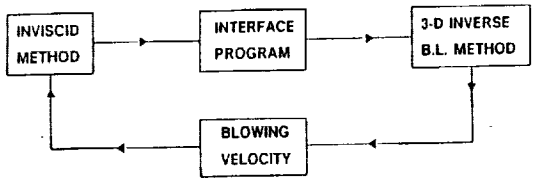

Fig. 4. The interactive boundary-layer method.

The above procedure is appropriate to wings without ice and has been used to compute transonic flows on wing/body configurations[18] where, since the wing leading edge was free of ice, there was no difficulty in generating solutions near the attachment line by constructing the nonorthogonal coordinate system and computing the geometrical properties of the wing. For a wing with ice, generation of the boundary-layer solutions near the leading edge can pose problems since the geodesic curvatures and metric coefficients must be determined for an irregular surface. In addition, the formulation of the interactive boundary-layer method developed for iced airfoils must take account of the three-dimensional nature of the flow. Thus, it is necessary to make changes in the strategy for solving the three-dimensional boundary-layer equations for an iced wing. These are considered below.

4.1 Boundary-Layer Equations

The three-dimensional boundary-layer equations for a nonorthogonal coordinate system are given in several references (for example, Ref. 26). With Reynolds stresses modeled by the eddy-viscosity concept, they can be written as,

$$\frac{\partial}{\partial x}(uh_2\sin\theta) + \frac{\partial}{\partial z}(wh_1\sin\theta) + \frac{\partial}{\partial y}(vh_1h_2\sin\theta) = 0 \tag{26}$$

$$\frac{u}{h_1}\frac{\partial u}{\partial x} + \frac{w}{h_2}\frac{\partial u}{\partial z} + v\frac{\partial u}{\partial y} - K_1u^2\cot\theta + K_2w^2\operatorname{cosec}\theta + K_{12}uw = -\frac{\operatorname{cosec}^2\theta}{\rho h_1}\frac{\partial p}{\partial x} + \frac{\cot\theta\,\operatorname{cosec}\theta}{\rho h_2}\frac{\partial p}{\partial z} + \nu\frac{\partial}{\partial y}\left(b\frac{\partial u}{\partial y}\right) \tag{27}$$

$$\frac{u}{h_1}\frac{\partial w}{\partial x} + \frac{w}{h_2}\frac{\partial w}{\partial z} + v\frac{\partial w}{\partial y} - K_2w^2\cot\theta + K_1u^2\operatorname{cosec}\theta + K_{21}uw = \frac{\cot\theta\,\operatorname{cosec}\theta}{\rho h_1}\frac{\partial p}{\partial x} - \frac{\operatorname{cosec}^2\theta}{\rho h_2}\frac{\partial p}{\partial z} + \nu\frac{\partial}{\partial y}\left(b\frac{\partial w}{\partial y}\right) \tag{28}$$

Here x denotes the coordinate along the lines formed by the intersection of the wing surface and planes representing constant percent semispan; z is the coordinate along the constant percent chordlines that generate the wing surface, with chord defined as the maximum length line between leading edge and trailing edge. The third coordinate y denotes the direction normal to the wing surface, and the parameter h denotes the metric coefficients, with θ the angle between the coordinate lines x = const and z = const. For an orthogonal system, $\theta = \pi/2$. The parameters K_1 and K_2 are known as the geodesic curvatures of the curves z = const and x = const, respectively. Equations (26) to (28) are subject to the following boundary conditions

$$y = 0, \quad u = 0, \quad v = 0, \quad w = 0 \tag{29a}$$

$$y = \delta, \quad u = u_e(x,z), \quad w = w_e(x,z) \tag{29b}$$

The solution of the above equations also requires initial conditions on two intersecting planes; those in the (y,z) plane at a specified chordwise location are determined from the solutions of the equations discussed in Subsection 4.3. Those on the (x,y) plane, at a specified spanwise location $z = z_o$, with z_o corresponding to, say, the root location, are determined from the solutions of the quasi-three-dimensional form of Eqs. (26) to (28) with all derivatives with respect to z neglected, that is,

$$\frac{\partial}{\partial x}(uh_2\sin\theta) + \frac{\partial}{\partial y}(vh_1h_2\sin\theta) = 0 \tag{30}$$

$$\frac{u}{h_1}\frac{\partial u}{\partial x} + v\frac{\partial u}{\partial y} - K_1u^2\cot\theta + K_2w^2\operatorname{cosec}\theta + K_1uw = -\frac{\operatorname{cosec}^2\theta}{\rho h_1}\frac{\partial p}{\partial x} + \nu\frac{\partial}{\partial y}\left(b\frac{\partial u}{\partial y}\right) \tag{31}$$

$$\frac{u}{h_1}\frac{\partial w}{\partial x} + v\frac{\partial w}{\partial y} - K_2w^2\cot\theta + K_1u^2\operatorname{cosec}\theta + K_{21}uw = \frac{\cot\theta\,\operatorname{cosec}\theta}{\rho h_1}\frac{\partial p}{\partial x} + \nu\frac{\partial}{\partial y}\left(b\frac{\partial w}{\partial y}\right) \tag{32}$$

subject to the same boundary conditions given in Eq. (29).

4.2 Interaction Law

To account for possible flow separation, as in two-dimensional flows, we use the interaction law of Veldman[27] where, for airfoil flows, the edge velocity is expressed as the sum of an inviscid velocity $u_e^0(x)$ and perturbation velocity $\delta u_e(x)$ due to viscous effects, that is,

$$u_e(x) = u_e^0(x) + \delta u_e(x) \tag{33}$$

The perturbation velocity is given by the Hilbert integral

$$\delta u_e(x) = \frac{1}{\pi} \int_{x_a}^{x_b} \frac{d}{d\sigma} (u_e \delta^*) \frac{d\sigma}{x - \sigma} \qquad (34)$$

in the interaction region (x_a, x_b).

To extend this inverse formulation to three-dimensional flows, it is necessary that the two-dimensional interaction formula given by Eq. (34) be either modified to account for the interaction in the x- and z-directions or be replaced by another formulation which provides a relationship between displacement surface and external velocity. Here we use the former approach, as described in Ref. 18, and first generate an initial displacement surface by solving the quasi-three-dimensional boundary-layer equations subject to the boundary conditions given by Eqs. (29) and (33) with the external velocity distribution $u_e^0(x)$ obtained from the panel method. The second step involves interaction between the inviscid flow equations and the quasi-three-dimensional flow equations. As in two-dimensional flows, the solutions of the boundary-layer equations are used to compute distributions of blowing velocity on the surface, and these allow the inviscid flow solutions to be updated. In step three, after the calculation of the initial conditions in the (y,z) and (x,y) planes, the fully three-dimensional boundary-layer equations are solved with the external velocity components resulting from step two. As before, the spanwise velocity component is assumed to correspond to its inviscid value. The viscous flow solutions are obtained by marching in the spanwise direction at each advancing chordwise location. This represents the first phase in an interactive loop that involves the fully three-dimensional boundary-layer equations. In the subsequent phases, as before, the blowing velocity distribution is used to obtain improved inviscid flow solutions, so the fully three-dimensional boundary-layer equations are solved for iced wings as for clean wings in transonic flow.[18]

The viscous effects in the spanwise component w_e are assumed to be second order, although their neglect is contrary to the irrotationality condition. However, trial calculations involving variations of both velocity conditions showed that errors were smaller than those associated with the convergence of the solutions.

4.3 Transformed Equations

As in two-dimensional flows, we express the boundary-layer equations in transformed variables for computational purposes. At first, when the equations are solved for a prescribed external velocity distribution (standard problem), we use the Falkner-Skan transformation and a modified version of this transformation for the inverse mode. In the former case, the independent variables are defined by

$$x = x, \quad z = z, \quad \eta = \left(\frac{u_e}{\nu s}\right)^{1/2} y, \quad s = \int_0^x h_1 dx \qquad (35)$$

For the dependent variables u, v and w, we introduce a two-component vector potential such that

$$u h_2 \sin\theta = \frac{\partial \psi}{\partial y}, \quad w h_1 \sin\theta = \frac{\partial \Phi}{\partial y},$$

$$v h_1 h_2 \sin\theta = -\left(\frac{\partial \psi}{\partial x} + \frac{\partial \Phi}{\partial z}\right) \qquad (36)$$

In addition, dimensionless parameters f and g are defined by

$$\psi = (u_e \nu s)^{1/2} h_2 \sin\theta f(x,z,\eta)$$

$$\Phi = (u_e \nu s)^{1/2} \frac{u_o}{u_e} h_1 \sin\theta g(x,z,\eta) \qquad (37)$$

$$(bf'')' + ef'' + m_2 (f')^2 + m_5 f'g' + m_8 (g')^2 + m_{11} = m_{10} f' \frac{\partial f'}{\partial x} + m_7 g' \frac{\partial f'}{\partial z} \qquad (38)$$

$$(bg'')' + eg'' + m_4 f'g' + m_3 (g')^2 + m_9 (f')^2 + m_{12} = m_{10} f' \frac{\partial g'}{\partial x} + m_7 g' \frac{\partial g'}{\partial z} \qquad (39)$$

$$e' = m_1 f' + m_6 g' + m_{10} \frac{\partial f'}{\partial x} + m_7 \frac{\partial g'}{\partial z} \qquad (40)$$

The coefficients m_1 to m_{12} are defined by

$$m_1 = (\sqrt{u_e s}\, h_2 \sin\theta)^{-1} \frac{s}{h_1} \frac{\partial}{\partial x} (\sqrt{u_e s}\, h_2 \sin\theta)$$

$$m_2 = -\frac{s}{u_e h_1} \frac{\partial u_e}{\partial x} + s K_1 \cot\theta, \quad m_3 = s K_2 \frac{u_o}{u_e} \cot\theta,$$

$$m_4 = -s K_{21}, \quad m_5 = -\frac{s}{u_e^2} \frac{u_o}{h_2} \frac{\partial u_e}{\partial z} - s K_{12} \frac{u_o}{u_e},$$

$$m_6 = (\sqrt{u_e s}\, h_1 \sin\theta)^{-1} \frac{s}{h_2} \frac{\partial}{\partial z} \left(\sqrt{u_e s}\, h_1 \sin\theta \frac{u_o}{u_e}\right) \qquad (41)$$

$$m_7 = \frac{s u_o}{h_2 u_e}, \quad m_8 = -s K_2 \left(\frac{u_o}{u_e}\right)^2 \csc\theta,$$

$$m_9 = -s K_1 \frac{u_e}{u_o} \csc\theta, \quad m_{10} = \frac{s}{h_1}$$

$$m_{11} = -\left[m_2 + m_5 \frac{w_e}{u_o} + m_8 \left(\frac{w_e}{u_o}\right)^2\right],$$

$$m_{12} = -\left[m_3 \left(\frac{w_e}{u_o}\right)^2 + m_4 \left(\frac{w_e}{u_o}\right) + m_9\right] + m_{13}$$

$$m_{13} = \frac{m_{10}}{u_o} \frac{\partial w_e}{\partial x} + m_7 \frac{w_e}{u_o^2} \frac{\partial w_e}{\partial z}$$

In terms of transformed variables, boundary conditions given by Eq. (29) become

$$\eta = 0: \quad f = g = f' = g' = 0$$

$$\eta = \eta_e: \quad f' = 1, \quad g' = \frac{w_e}{u_o} \qquad (42)$$

The form of the transformed quasi-three-dimensional equations (Eqs. (30) - (32)) is identical to the form of Eqs. (38) to (40), except that

$$\frac{\partial f'}{\partial z} = \frac{\partial g'}{\partial z} = \frac{\partial u_e}{\partial z} = \frac{\partial w_e}{\partial z} \equiv 0 \qquad (43a)$$

and m_5 and m_6 are now defined by:

$$m_5 = -K_{12} s \frac{u_o}{u_e}, \qquad m_6 \equiv 0 \qquad (43b)$$

To solve the equations in the inverse mode, we define independent variables by

$$x = x, \quad z = z, \quad Y = \left(\frac{u_o}{\nu s}\right)^{1/2} y, \quad s = \int_0^x h_1 dx \qquad (44)$$

and relate the vector potentials ψ and Φ to f and g by

$$\psi = (u_o \nu s)^{1/2} h_2 \sin\theta f(x,z,\eta)$$
$$\Phi = (u_o \nu s)^{1/2} h_1 \sin\theta g(x,z,\eta) \qquad (45)$$

and with a prime now denoting differentiation with respect to Y and u_e and w_e denoting edge velocity components normalized by reference velocity u_o, Eqs. (26) to (28), with e' defined by Eq. (40), are written as

$$(bf'')' + ef'' + m_2[(f')^2 - (\bar{u}_e)^2] + m_5[f'g' - \bar{u}_e\bar{w}_e] + m_8[(g')^2 - (\bar{w}_e)^2] = m_{10}(f' \frac{\partial f'}{\partial x} - \bar{u}_e \frac{\partial \bar{u}_e}{\partial x}) + m_7(g' \frac{\partial f'}{\partial z} - \bar{w}_e \frac{\partial \bar{u}_e}{\partial z}) \qquad (46)$$

$$(bg'')' + eg'' + m_3[(g')^2 - (\bar{w}_e)^2] + m_4[f'g' - \bar{u}_e\bar{w}_e] + m_9[(f')^2 - (\bar{u}_e)^2] = m_{10}(f' \frac{\partial g'}{\partial x} - \bar{u}_e \frac{\partial \bar{w}_e}{\partial x}) + m_7(g' \frac{\partial g'}{\partial z} - \bar{w}_e \frac{\partial \bar{w}_e}{\partial z}) \qquad (47)$$

The coefficients m_1 to m_{10} are now given by

$$m_1 = \frac{s^{1/2}}{h_1 h_2 \sin\theta} \frac{\partial}{\partial x}(s^{1/2} h_2 \sin\theta), \quad m_2 = sK_1\cot\theta,$$
$$m_3 = sK_2\cot\theta, \quad m_4 = -sK_{21}, \quad m_5 = -sK_{12},$$
$$m_6 = \frac{s^{1/2}}{h_1 h_2 \sin\theta} \frac{\partial}{\partial z}(s^{1/2} h_1 \sin\theta) \qquad (48)$$
$$m_7 = s/h_2, \quad m_8 = -sK_2\csc\theta,$$
$$m_9 = -sK_1\csc\theta, \quad m_{10} = s/h_1$$

The transformed boundary conditions for the system of Eqs. (46) and (47), with u_e given by Eq. (33) and with w_e corresponding to its inviscid value, are

$$\eta = 0: \quad f = g = f' = g' = 0 \qquad (49a)$$

$$\eta = \eta_e: \quad f' = \bar{u}_e, \quad g' = \bar{w}_e \qquad (49b)$$

The quasi-three-dimensional form of the equations, which are subject to the boundary conditions given by Eq. (49), are obtained from the above equations by setting

$$\frac{\partial f'}{\partial z} = \frac{\partial g'}{\partial z} = \frac{\partial \bar{u}_e}{\partial z} = \frac{\partial \bar{w}_e}{\partial z} = 0 \quad \text{and} \quad m_6 = 0 \qquad (50)$$

To generate the initial conditions near the leading edge of the iced wing, we use quasi-three-dimensional boundary-layer equations expressed in the inverse mode given by

$$(bf'')' + ef'' + m_2[(f')^2 - (\bar{u}_e)^2] + m_5(f'g' - \bar{u}_e\bar{w}_e) + m_8[(g')^2 - (\bar{w}_e)^2] = m_{10}(f' \frac{\partial f'}{\partial x} - \bar{u}_e \frac{\partial \bar{u}_e}{\partial x}) \qquad (51)$$

$$(bg'')' + eg'' + m_3[(g')^2 - (\bar{w}_e)^2] + m_4(f'g' - \bar{u}_e\bar{w}_e) + m_9[(f')^2 - (\bar{u}_e)^2] = m_{10}(f' \frac{\partial g'}{\partial x} - \bar{u}_e \frac{\partial \bar{w}_e}{\partial x}) \qquad (52)$$

$$e' = m_1 f' + m_{10} \frac{\partial f'}{\partial x} \qquad (53)$$

The above equations can be further simplified if we assume that two adjacent defining sections of a wing are connected by straight line development, as commonly used in the wing design. This feature simplifies the problem of shaping the metal for a wing surface. As a consequence, we can neglect the geodesic curvature of x = constant lines, namely K_2, and thus set $m_3 = m_8 = 0$. From the definitions of m_4 and m_5, it can be seen that as a result of the above assumption, these two terms are also small and can be neglected. We further assume that the local variations in cross sections in the spanwise direction are small. Examination of the terms m_1, m_2 and m_9 for a typical wing shows that m_2 reaches a value less than 0.1 very close to the leading edge ($x/c < 0.01$) and m_9 reaches a maximum value of 0.2. However, their magnitudes rapidly decrease with increasing x and reach a very small value at $x/c < 0.1$. This behavior allows us to neglect m_2 and m_9 in the equations and set $m_1 = 1/2$.

4.4 Solution Procedure

A detailed description of the solution procedure will be reported later separately. Briefly, the boundary-layer equations expressed in terms of transformed variables are solved with Keller's two-point finite-difference method[26] (box scheme) with boundary conditions expressed in inverse form with the interaction law described in Subsection 4.2. Depending on the complexity of the flowfield, two forms of the box scheme are employed. In regions where all velocity components are positive, the regular box scheme is used. In regions of either a negative spanwise velocity component or

negative streamwise velocity component, the zig-zag box scheme described in Ref. 26 is used.

5.0 Comparison of Calculated and Measured Ice Shapes on a Swept Wing

The approach described in Section 3 was applied to the calculation of ice shapes that have been observed on a MS-317 swept wing obtained under infinite swept wing conditions. These data were also used for a similar purpose by Potapczuk and Bidwell[25], as discussed in Section 3.

In general, the infinite yawed wing conditions apply to the mid-semispan section of wings with an aspect ratio greater than about five. This approximation becomes progressively less accurate as the tip or the root of the wing is approached but in most instances it can still provide reasonable answers. A point to remember about the use of this approximation with finite aspect ratio wings is that although the flow may have the desired characteristics, its lift is always less than the lift of a wing with infinite aspect ratio. This may lead to problems in comparing calculations with experimental data unless the aspect ratio or the pressure distribution is also given. If the pressure distribution is not available, the given angle of attack may not properly represent the experimental conditions. Similar problems may also arise in simulating wind-tunnel conditions by calculating the corrected incidence and lift coefficient in free air, because the trajectories in the two cases may be far from identical. One solution to the wind-tunnel problem, which may be the only acceptable solution for a swept wing spanning the tunnel, is to calculate the flowfield about the wing in the presence of the tunnel walls. This is within the capability of the inviscid method discussed in Section 2, and studies are underway using this capability to investigate the effect of wind tunnel walls on the pressure distribution.

The comparisons presented here are for the test conditions given in Table 1. Additional studies for other test conditions are in progress and will be reported later. The calculated ice shapes in Figures 5 and 6 were obtained for the untapered wing with a MS-317 airfoil section defined streamwise with a sweep angle of 30° and an aspect ratio of six. All trajectory and ice accretion calculations were carried out with inviscid flow computed on the mid-semispan section where the spanwise pressure gradient was negligible. All calculations were performed for one time step to save computer time, which is approximately 7 minutes per run on the Cray computer. The increase in time, in comparison with the two-dimensional case, is primarily due to the trajectory calculations where, despite the yawed infinite wing approximations, the computation of the off-body velocities involves repeated large matrix multiplications in which all wing panels are represented.

Table 1. Test Conditions for MS-317 Ice Accretion Experiment of Ref. 8, V_∞ = 150 mph, d = 20 μm, LWC = 1.03 gm^{-3}.

Run	T_∞ (°F)	t (sec)	α (deg)	$(k_s/c)_1$
1	15	1164	2.0	0.00192
6	15	1164	8.0	0.00192
7	15	390	2.0	0.00192
8	0	390	2.0	0.00127
9	0	390	8.0	0.00127
10	0	1164	8.0	0.00127
11	0	1164	2.0	0.00127

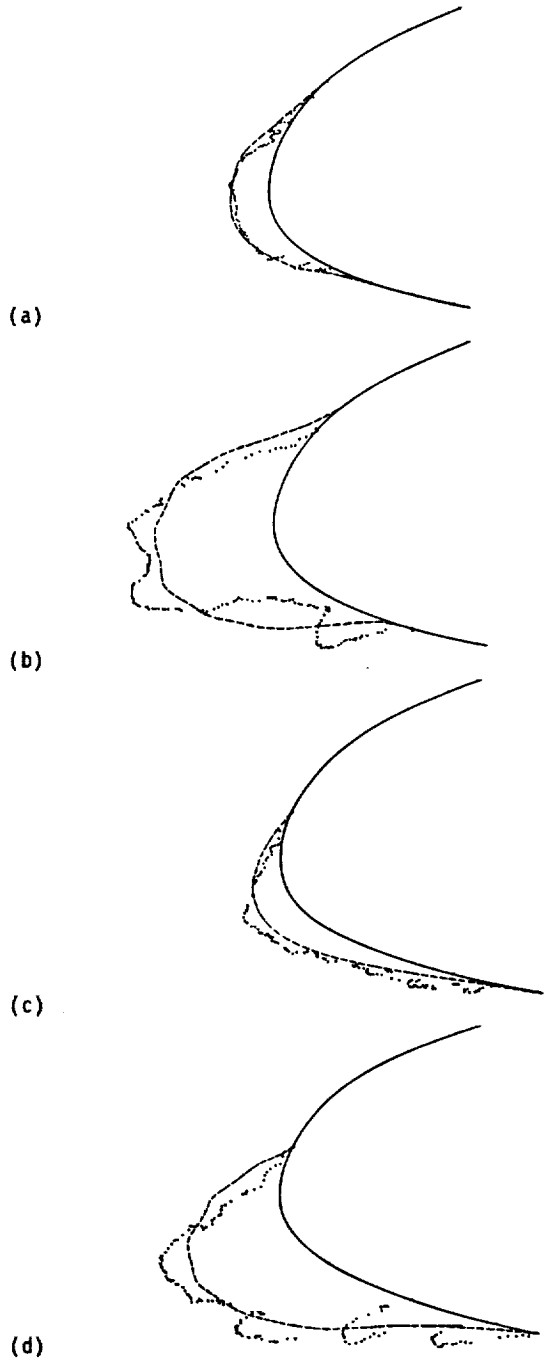

Fig. 5. Comparison of calculated (solid lines) and measured (dashed lines) ice shapes. Rime ice: (a) Run 8, (b) Run 11, (c) Run 9, (d) Run 10.

Figure 5a shows a comparison of measured and calculated ice shapes for Run 8 which corresponds to T_∞ = 0°, α = 2°, t = 390 sec. As can be seen, the agreement between measured and calculated results is remarkably good. The calculated results for a calculation time of 1164 sec and for T_∞ = 0°F and α = 2° (Run 11) are shown in Fig. 5b and indicate reasonable agreement with measurements despite the one time step used in the calculations. It is

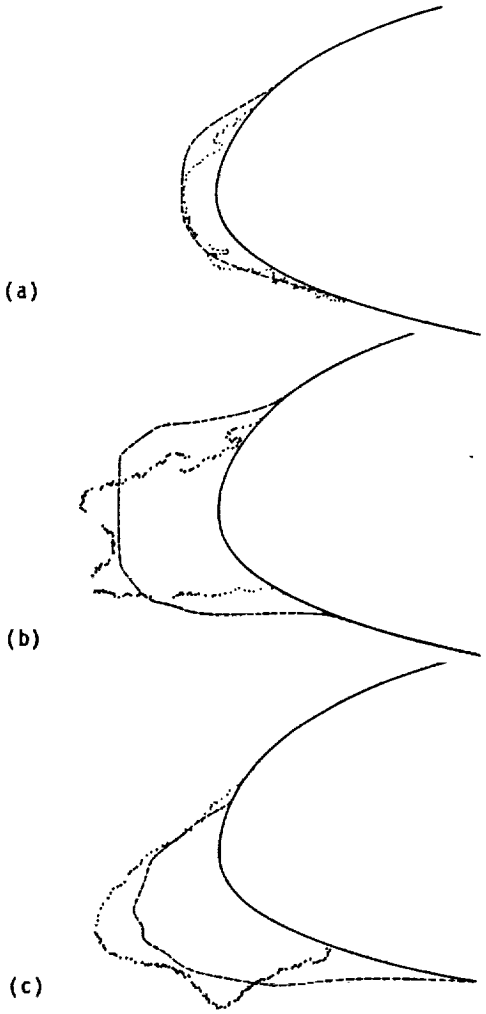

Fig. 6. Comparison of calculated (solid lines) and measured (dashed lines) ice shapes. Mixed ice: (a) Run 7, (b) Run 1, (c) Run 6.

expected that the ice growth will have some effect on the velocity field and on the calculated droplet impingement. A comparison of predicted and measured ice shapes obtained for $T_\infty = 0°F$ at $\alpha = 8°$ for t = 390 and 1164 sec. (Runs 9 and 10) are shown in Figs. 5c and 5d, respectively. The agreement is again reasonable, keeping in mind that only one time step was used in the calculations.

The next set of studies was conducted for a slightly higher freestream temperature of T_∞ = 15°F, representing an icing condition for which a mixed ice growth was observed. Run 7 in Fig. 6a for $\alpha = 2°$ and t = 390 sec. indicates good agreement between experiment and theory, except for some deviation on the upper surface. The results in Fig. 6b at the large time step of t = 1164 sec. (Run 1) are more or less in agreement in predicting the amount of ice accumulated, but they differ in predicting its shape. It is known from two-dimensional calculations that a large number of relatively short time steps are needed to predict horn-shaped ice for glaze ice. Since the mixed ice formation tends toward glaze ice shapes for large times, it is not surprising that one time step calculation is not sufficient to predict the actual growth of the ice shapes. Similar comments apply to Fig. 6c, where comparisons are for a large time step of t = 1164 sec. (Run 6), but at $\alpha = 8°$.

6.0 Performance Degradation of an Iced Tapered Wing

The interactive boundary-layer method of Section 4 was used to study the performance degradation of an iced wing having MS-317 airfoil streamwise sections, an aspect ratio of 3.43, and a taper ratio of 0.4. Icing conditions were chosen to correspond to those in Runs 8 and 11, shown in Table 1. The pressure distribution on the wing was computed at four locations defined by the midsection of each wing-section with a hundred panels on each defining airfoil section. The ice shapes corresponding to this pressure distribution were computed with the method of Section 3 in the middle of each wing section and were used to distribute ice along the leading edge of the tapered wing. The computed ice shapes for $\alpha = 2°$ were then assumed to be the same for all angles of attack on the wing in the investigation of the performance degradation of the wing due to ice shapes corresponding to the atmospheric conditions given in Runs 8 and 11. At a specified angle of attack, with the defined ice shapes along the leading-edge of the wing, calculations were performed with the method of Section 4; that is, inviscid flow calculations performed for an iced wing were followed by the inverse three-dimensional boundary-layer calculations to determine the blowing velocity distribution to be used in the incorporation of viscous effects into the inviscid method. The inviscid flow solutions made use of four lifting strips, and the viscous flow calculations included boundary-layer calculations on the wing and in the wake, the latter requiring velocities at off-body points in the potential field. This interactive and iterative procedure was repeated until the solutions converged. The lift coefficients were then calculated from the inviscid method for each individual strip and included the contribution of ice protruding beyond the wing contour and the drag coefficients from the boundary-layer calculations.

Figure 7 shows the variation of the calculated lift coefficients as a function of angle of attack. Since the primary purpose of the calculations was to demonstrate the increase in drag due to ice on a tapered wing, the angle of attack range was not extended to stall, which would occur at relatively high angles of attack for low aspect ratio wings. The higher lift coefficient than for the clean wing shown for the two iced wings is due to the normalization with the wing area of the clean wing in both cases. The conclusion from this figure is that lift is not affected by the rime ice accretion

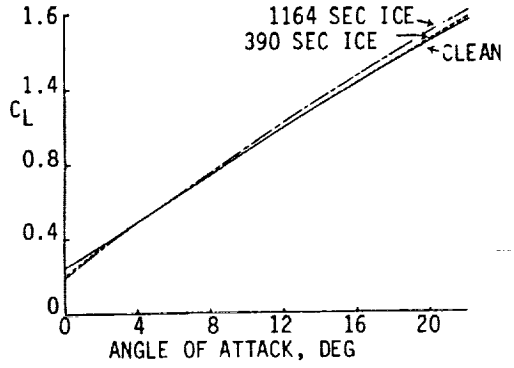

Fig. 7. Effect of leading-edge 390 and 1164 second rime ice on the lift coefficient of a tapered wing for $R = 4.6 \times 10^6$ based on root chord.

for the angle of attack range considered here because the ice shapes along the leading edge of the wing for runs 8 and 11 do not cause premature flow separation on the wing.

The calculated drag coefficients shown in Fig. 8 represent the profile drag of the wing only and do not represent the total drag, since that requires the contribution of the induced drag. The profile drag was calculated sectionwise from the Squire-Young formula based on the resultant velocity at the trailing edge. Comparable results were also obtained from the momentum deficiency in the far wake. Here we see considerable differences between the clean wing and the two iced wings because the Reynolds number is relatively low (Re = 4.6 x 10^6 for the root chord) and there are large regions of laminar flow on the clean wing. The principal contributor to the drag increase for the iced wing is the shift in transition to near the leading edge due to roughness of the iced surface. The contribution of the surface roughness itself to the drag is very small for Run 8 because the extent of ice is small and its shape emulates an airfoil leading edge. The additional drag increase for Run 11 results from the surface roughness spread over a large wetted area increment. The main conclusion that can be drawn from these comparisons is that drag increments obtained between clean and iced airfoils in wind tunnels depend on transition locations on the clean wing. If the Run 8 case represents a wing with transition fixed at the leading edge and the clean wing case is transition free, the observed drag increments from the Run 11 case are quite different from each other. As a corollary, drag increments obtained from wind-tunnel tests may be meaningless without fixing transition or knowing where transition occurs during the tests.

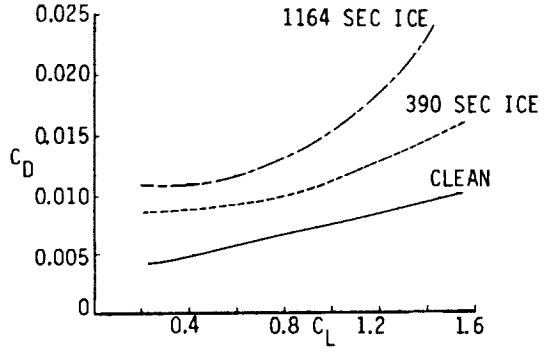

Fig. 8. Effect of leading edge 390 and 1164-second rime ice on the profile drag coefficient of a tapered wing for R_c = 4.6 x 10^6 based on root chord.

7.0 Concluding Remarks

A method for predicting ice accretion along the leading edge of a wing is described and evaluated by comparing calculated results with experimental data for several atmospheric icing conditions obtained on a MS-317 wing with infinite swept-wing conditions. Overall, calculated ice shapes are in good agreement with measurements.

A method is also described for computing the aerodynamic properties of clean and iced wings. This method is based on the extension of the interactive boundary-layer method previously developed for clean and iced airfoils. It is applied to a tapered with wing leading edge rime ice accretion of 390 and 1164 seconds to study the wing performance degradation for a range of angles of attack less than stall at a root-chord Reynolds number of 4.6 x 10^6. Calculated lift coefficients indicate that the lift is not affected by the rime ice accretion because the leading-edge ice shapes do not cause premature flow separation on the wing for the atmospheric icing conditions and angle of attack range considered in the study. Calculated profile drag coefficients for clean and iced wings, on the other hand, show the expected differences; that is, the increase in drag due to leading-edge ice. The main reason for the drag increase is the movement of the transition locations to the wing leading edge due to the roughness of the iced surface. The contribution of the surface roughness to the drag is relatively small for the small ice accumulated for 390 seconds because the extent of ice is small. For an ice shape corresponding to 1164 seconds, however, the drag increase is more pronounced because, in this case, the surface roughness spreads over a larger wetted area increment.

Both methods for predicting ice shapes along the wing leading edge and for computing its aerodynamic performance degradation due to icing are very encouraging. The methods are general and can be applied to other parts of an airplane other than a wing, including the engine intakes. Studies are currently underway to apply these methods to determine the performance degradation of a typical twin-engine commuter-type aircraft in measured natural icing conditions.

8.0 References

1. National Aircraft Icing Plan. Federal Coordination for Meteorological and Supporting Services, Department of Commerce, FCM P20-1986, April 1986.

2. MacArthur, C.D., Keller, J.L. and Leurs, J.K., "Mathematical Modeling of Ice Accretion of Airfoils," AIAA Paper 82-0284, 1982.

3. Ruff, G.A. and Berkowitz, B.M., "User's Manual for the NASA Lewis Ice Accretion Code (LEWICE)," NASA CR-185129, May 1990.

4. Cebeci, T., "Calculation of Flow Over Iced Airfoils," AIAA J., Vol. 27, p. 853, 1989.

5. Potapczuk, M.G., "Navier-Stokes Analysis of Airfoils with Leading-Edge Ice Accretions," Ph.D. Dissertation, The University of Akron, May 1989.

6. Cebeci, T. Chen, H.H. and Alemdaroglu, N., "Fortified LEWICE with Viscous Effects," Journal of Aircraft, Vol. 28, No. 9, pp. 564-571, Sept. 1991.

7. Olsen, W., Shaw, R. and Newton, J., "Ice Shapes and the Resulting Drag Increase for a NACA 0012 Airfoil," NASA TM 83556, Jan. 1984.

8. Bidwell, C.S., "Icing Characteristics of a Natural Laminar Flows, a Medium-Speed, and a Swept Medium-Speed Airfoil," AIAA Paper 91-0447, Jan. 1991.

9. Federal Aviation Regulations Parts 25, 27 and 29, "Airworthiness Standards: Transportation Category Airplanes, Normal Category Rotorcraft, and Transport Category Rotorcraft. Appendix C., Washington D.C. 20591, Department of Transportation Federal Aviation Admin., 1974.

10. Bragg, M., Khodadoust, A., Soltani, R., Wells, S. and Kenko, M., "Effect of a Simulated Ice Accretion on the Aerodynamics of a Swept Wing," AIAA Paper 91-0442, 1991.

11. Bragg, M.B.and Coirier, W.J., "Aerodynamic Measurements of an Airfoil with Simulated Glaze Ice," AIAA Paper 86-0484, Jan. 1986.

12. Bragg, M.B. and Spring, S.A., "An Experimental Study of the Flowfield about an Airfoil with Glaze Ice," AIAA Paper 87-0100, Jan. 1987.

13. Bragg, M.B. and Khodadoust, A., "Experimental Measurements in a Large Separation Bubble Due to a Simulated Glaze Ice Accretion," AIAA Paper 88-0116, Jan. 1988.

14. Kwon, O.J. and Sankar, L.N., "Numerical Study of the Effects of Icing on Finite Wing Aerodynamics," AIAA Paper 90-0757, 1990.

15. Kwon, O.J. and Sankar, L.N., "Numerical Study of the Effect of Icing on Fixed and Rotary Wing Performance," AIAA Paper 91-0662, 1991.

16. Berkowitz, B.M. and Riley, J.T., "Analytical Ice Shape Predictions for Flight in Natural Icing Conditions," NASA CR-182234, 1989.

17. Shin, J., Berkowitz, B., Chen, H.H. and Cebeci, T., "Prediction of Ice Shapes and Their Effect on Airfoil Performance," AIAA Paper 91-0264, Jan. 1991.

18. Cebeci, T., Khattab, A.A., Chen, H.H. and Chen, L.T., "An Approach to the Design of Wings: The Role of Mathematics, Physics and Economics," AIAA Paper No. 92-0286, Jan. 1992.

19. Hess, J.L., "The Problem of Three-Dimensional Lifting Flow and Its Solution by Means of Surface Singularity Distribution," Computer Methods in Applied Mechanics and Engineering, Vol. 4, pp. 283-319, 1974.

20. Margason, R.J., Kjelgaard, S.O., Sellars, W.L., III, Morris, C.E.K., Jr., Walkley, K.B. and Shields, E.W., "Subsonic Panel Methods - A Comparison of Several Production Codes," AIAA Paper 85-0280, 1985.

21. Olsen, W. and Walker, E., "Close Up Motion Pictures of the Icing Process," NASA Lewis Research Center Film, 1983.

22. Olsen, W. and Walker, E., "Experimental Evidence for Modifying the Current Physical Model for Ice Accretion on Aircraft Structures," NASA TM 87184, May 1986.

23. Hansman, R.,J. and Turnock, S.R., "Investigation of Surface Water Behavior During Glaze Ice Accretion," Journal of Aircraft, Vol. 26, No. 2, p. 140, Feb. 1989.

24. Bilanin, A.J., "Proposed Modification to Ice Accretion/Ice Scaling Theory," Journal of Aircraft, Vol. 28, No. 6, p. 353, June 1991.

25. Potapczuk, M.G. and Bidwell, C.S., "Numerical Simulation of Ice Growth on a MS-317 Swept Wing Geometry," AIAA Paper No. 91-0263, 1991.

26. Bradshaw, P., Cebeci, T. and Whitelaw, J.H., Engineering Calculation Methods for Turbulent Flows, Academic Press, London, 1981.

27. Veldman, A.E.P., "New Quasi-Simultaneous Method to Calculate Interacting Boundary Layers," AIAA Journal, Vol. 19, p. 679, 1981.

0749c

REPORT DOCUMENTATION PAGE

Form Approved
OMB No. 0704-0188

1. AGENCY USE ONLY (*Leave blank*)	2. REPORT DATE	3. REPORT TYPE AND DATES COVERED
	January 1992	Technical Memorandum

4. TITLE AND SUBTITLE
Analysis of Iced Wings

5. FUNDING NUMBERS
WU-505-68-10

6. AUTHOR(S)
T. Cebeci, H.H. Chen, K. Kaups, S. Schimke, and J. Shin

7. PERFORMING ORGANIZATION NAME(S) AND ADDRESS(ES)
National Aeronautics and Space Administration
Lewis Research Center
Cleveland, Ohio 44135-3191

8. PERFORMING ORGANIZATION REPORT NUMBER
E-7201

9. SPONSORING/MONITORING AGENCY NAMES(S) AND ADDRESS(ES)
National Aeronautics and Space Administration
Washington, D.C. 20546-0001

10. SPONSORING/MONITORING AGENCY REPORT NUMBER
NASA TM-105773

11. SUPPLEMENTARY NOTES
Prepared for the 30th Aerospace Sciences Meeting and Exhibit sponsored by the American Institute of Aeronautics and Astronautics, Reno, Nevada, January 6-9, 1992. T. Cebeci, H.H. Chen, K. Kaups, S. Schimke, Aerospace Engineering Department, California State University, Long Beach, Long Beach, California 90801. J. Shin, NASA Lewis Research Center, Cleveland, Ohio. Responsible person, J. Shin, (216) 433-8714.

12a. DISTRIBUTION/AVAILABILITY STATEMENT
Unclassified - Unlimited
Subject Category 02

12b. DISTRIBUTION CODE

13. ABSTRACT ***(Maximum 200 words)***

A method for computing ice shapes along the leading edge of a wing and a method for predicting its aerodynamic performance degradation due to icing is described. Ice shapes are computed using an extension of the LEWICE code which was developed for airfoils. The aerodynamic properties of the iced wing are determined with an interactive scheme in which the solutions of the inviscid flow equations are obtained from a panel method and the solutions of the viscous flow equations are obtained from an inverse three-dimensional finite-difference boundary-layer method. A new interaction law is used to couple the inviscid and viscous flow solutions. The application of the LEWICE wing code to the calculation of ice shapes on a MS-317 swept wing show good agreement with measurements. The interactive boundary-layer method is applied to a tapered ice wing in order to study the effect of icing on the aerodynamic properties of the wing at several angles of attack.

14. SUBJECT TERMS
Three-dimensional inverse boundary-layer method; Eddy-viscosity formulation; Swept wing

15. NUMBER OF PAGES
14

16. PRICE CODE
A03

17. SECURITY CLASSIFICATION OF REPORT	18. SECURITY CLASSIFICATION OF THIS PAGE	19. SECURITY CLASSIFICATION OF ABSTRACT	20. LIMITATION OF ABSTRACT
Unclassified	Unclassified	Unclassified	